ACS OMEGA

Article

Cite This: ACS Omega 2018, 3, 5654−5668

Microwave-Induced Synthesis of Chitosan Schiff Bases and Their Application as Novel and Green Corrosion Inhibitors: Experimental and Theoretical Approach

Jiyaul Haque,[†] Vandana Srivastava,*[,†] Dheeraj S. Chauhan,[‡] Hassane Lgaz,[§] and Mumtaz A. Quraishi*[,†,‡]

[†]Department of Chemistry, Indian Institute of Technology (Banaras Hindu University), Varanasi 221005, India

[‡]Center of Research Excellence in Corrosion, Research Institute, King Fahd University of Petroleum and Minerals, Dhahran 31261, Saudi Arabia

[§]Department of Applied Bioscience, College of Life & Environment Science, Konkuk University, 120 Neungdong-ro, Gwangjin-gu, Seoul 05029, South Korea

Supporting Information

ABSTRACT: Environmentally friendly three chitosan Schiff bases (CSBs) were first time synthesized under microwave irradiation by the reaction of chitosan and aldehydes [benzaldehyde (CSB-1), 4-(dimethylamino)benzaldehyde (CSB-2), and 4-hydroxy-3-methoxybenzaldehyde (CSB-3)] and characterized by IR and NMR spectroscopy. The corrosion inhibition performance of the synthesized inhibitors was studied by the electrochemical impedance spectroscopy (EIS) and potentiodynamic polarization (PDP). The results show that all the Schiff bases (CSBs) act as effective corrosion inhibitors for mild steel in 1 M HCl solution. Among the synthesized Schiff bases, CSB-3 exhibited the maximum inhibition efficiency of 90.65% at a very low concentration of 50 ppm. The EIS results showed that the CSBs inhibit corrosion by the adsorption mechanism. The PDP results show that all the three Schiff bases are mixed-type inhibitors. The formation of inhibitor films on the mild steel surface was supported by scanning electron microscopy/energy dispersive X-ray analysis and Fourier-transform infrared spectroscopy methods. The adsorption of CSBs on the mild steel surface obeys the Langmuir adsorption isotherm. The theoretical studies via density functional theory and molecular dynamics simulation corroborated the experimental results.

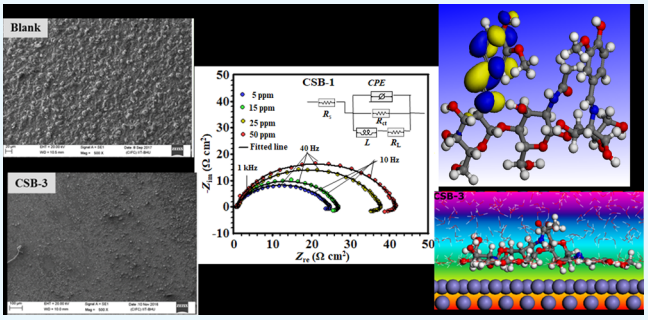

1. INTRODUCTION

Chitosan (N-deacetylated product of chitin) is a natural biopolymer composed of β-D-glucosamine and N-acetyl-β-D-glucosamine units with a 1,4-linkage. Chitosan is an attractive material because of its properties such as immunological activity, biocompatibility, low toxicity, and biodegradability.[1,2] Therefore, chitosan finds wide applications in medicine, cosmetics, textile, and many other industrial branches.[3−5] The anticorrosive nature of chitosan is attributed to the presence of $-NH_2$ and −OH groups through which it can coordinate with metal surfaces.[6] In addition to its biodegradability, chitosan has been reported as an environmentally benign corrosion inhibitor.[7,8]

Hydrochloric acid finds wide application in various industrial processes such as pickling, cleaning, descaling, and acidizing process of oil wells because of its low cost and effective cleaning action as compared to other mineral acids. The use of corrosion inhibitors is one of the best practical methods to reduce the corrosivity of the acid solutions. Organic compounds containing nitrogen, oxygen, phosphorus, and sulfur have been reported as corrosion inhibitors. They are adsorbed on the metal surface and block the active sites thereby retarding the corrosion reaction occurring on the metal surface.[9,10] Most of the organic compounds are toxic in nature. Therefore, the search for finding an eco-friendly corrosion inhibitor has received enormous attention. In this regard, chitosan and its derivatives have received much attention as corrosion inhibitors. In view of its eco-friendly nature, several authors have studied chitosan and its derivatives as corrosion inhibitors for various metals and alloys.[11−13]

One of the major drawbacks of chitosan and its earlier reported derivatives is poor solubility, which restricts its performance and renders it less effective. As far as ecological factors are considered, it would be beneficial to use environmentally friendly compounds for modification of the polymer matrix. The selection of chitosan Schiff bases (CSBs) as

Received: March 11, 2018
Accepted: May 15, 2018
Published: May 25, 2018

DOI: 10.1021/acsomega.8b00455
ACS Omega 2018, 3, 5654−5668

corrosion inhibitors is based on the fact that they are nontoxic and can be easily synthesized and insertion of imine linkage (−HC═N) in chitosan is likely to improve the anticorrosion performance and the film-forming capability. Recently, we synthesized chitosan-thiosemicarbazide and chitosan-thiocarbohydrazide and tested them as corrosion inhibitors in 1 M HCl, and good results were obtained. This prompted us to synthesize a few more chemically modified chitosan derivatives.[7,14] One of the important features of the work is that in the present work, we, herein for the first time, report the microwave-induced synthesis of Schiff bases of chitosan with benzaldehyde, *N*,*N*-dimethylaminobenzaldehyde, and *o*-hydroxyanisaldehyde. The use of microwave synthesis offers following benefits. It increases the rate of chemical reaction, yield of the product. The product is obtained in high purity without involving cumbersome purification steps.[15] The synthesized derivatives were characterized with Fourier-transform infrared (FTIR) and NMR studies. Their corrosion inhibition behavior on mild steel in hydrochloric acid has been investigated using gravimetric studies, electrochemical measurements and surface, analysis. Density functional theory (DFT)- and molecular dynamics (MD)-based theoretical studies have also been used to corroborate experimental results.

2. RESULTS AND DISCUSSION

2.1. Characterization of the Synthesized CSB Inhibitors. The FTIR spectra of the synthesized Schiff bases are displayed in Figure 1. The peaks at 1647, 1598, and 1646 cm^{-1}

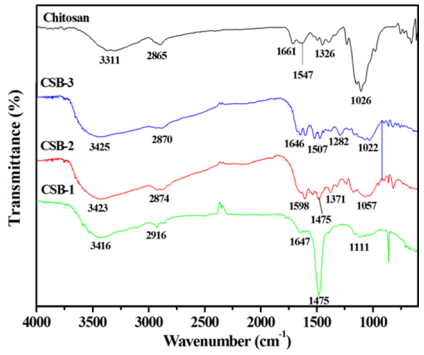

Figure 1. FTIR spectra of chitosan and synthesized CSBs.

correspond to the stretching vibration of −the C═N− bond of CSB-1, CSB-2, and CSB-3, respectively.[15] There is no characteristic peak of carbonyl group of free aldehydes in the region 1670−1820 cm^{-1}. These findings suggest the formation of Schiff bases, which was further confirmed by the NMR spectroscopy analysis, as shown in Figure S1. The details of FTIR and ^1H NMR spectra are given below:[16]

CSB-1, IR (ν_{max}/cm^{-1}, KBr): 3416 (−O−H), 2916 (═C−H), 1647 (−C═N−), 1475(−C═C−), 1111 (−C−O−). ^1H NMR (500 MHz, D_2O/CF_3COOD): δ_H 1.77 (Ac-H), 2.88−4.57 (H_1−H_6), 7.32−7.66 (5H, Ph), 9.63 (H_7),

CSB-2, IR (ν_{max}/cm^{-1}, KBr): 3423 (−O−H), 2874 (═C−H), 1598 (−C═N−), 1475(−C═C−), 1057 (−C−O−). ^1H NMR (500 MHz, D_2O/CF_3COOD): δ_H 1.34 (Ac-H), 2.59 (6H, Me), 2.45−4.14 (H_1−H_6), 7.07−7.37 (4H, Ph), 9.23 (H_7),

CSB-3, IR (ν_{max}/cm^{-1}, KBr): 3425 (−O−H), 2870 (═C−H), 1646 (−C═N−), 1507(−C═C−), 1022 (−C−O−). ^1H NMR (500 MHz, D_2O/CF_3COOD): δ_H 1.68 (Ac-H), 3.50 (3H, −OMe), 2.78−4.47 (H_1−H_6), 6.62−7.09 (3H, Ph), 9.26 (H_7).

2.2. Gravimetric Measurement. *2.2.1. Effect of Inhibitor Concentration and Immersion Time.* The results on the effect of varying concentrations of inhibitor on the corrosion of mild steel in 1 M HCl are listed in Table 1. It can be observed that

Table 1. Weight Loss Parameters Obtained for Mild Steel in 1 M HCl Containing Different Concentrations of CSBs

inhibitors	concn (ppm)	weight loss (mg)	C_R (mg cm^{-2} h^{-1})	surface coverage (θ)	IE (%)
blank	0.0	642	10.7		
CSB-1	5	145	2.42	0.7741	77.41
	15	108	1.80	0.8318	83.18
	25	96	1.60	0.8505	85.05
	50	86	1.43	0.8660	86.60
	100	73	1.22	0.8863	88.63
	150	74	1.23	0.8847	88.47
CSB-2	5	140	2.33	0.7819	78.19
	15	95	1.58	0.8520	85.20
	25	85	1.42	0.8676	86.76
	50	73	1.22	0.8876	88.76
	100	65	1.08	0.8987	89.87
	150	65	1.08	0.8987	89.87
CSB-3	5	120	2.00	0.8131	81.31
	15	90	1.50	0.8596	85.96
	25	81	1.35	0.8738	87.38
	50	60	1.00	0.9065	90.65
	100	55	0.92	0.9143	91.43
	150	53	0.88	0.9174	91.74

upon the addition of CSBs in the corrosive media, the corrosion rate (C_R) decreases significantly, while inhibition efficiency increases with increase in the inhibitor concentration, as a result of increase in the number of adsorbed inhibitor molecules over the active sites of the mild steel surface. However, above the 50 ppm of inhibitor concentration, IE was nearly constant, which suggests that 50 ppm concentration of CSBs is optimum for the protection of mild steel corrosion in 1 M HCl. Among the three Schiff bases, CSB-3 shows the highest IE of 90.65% at 50 ppm. The IE of these CSBs is in the order CSB-3 > CSB-2 > CSB-1. The difference in the corrosion inhibition behavior of CSBs can be explained on the basis of difference in the chemical structure of the investigated inhibitors as the difference in the inhibition performance of CSBs can be attributed to the presence of different substituent groups on the benzene ring. The CSB-3 has two substituents: $-OCH_3$ group at 3-position and −OH group at 4-position of the benzene ring, the CSB-2 has only one substituent: a dimethylamine group at the 4-position of the benzene ring, while CSB-1 has no substituents. These substituents have a lone pair of electrons on the heteroatom (oxygen, nitrogen), which increases the electron density of the benzene ring and enhances the inhibition efficiency of inhibitor molecules. These Schiff base derivatives of chitosan show a higher inhibition efficiency at a lower concentration than previously reported for chitosan and its derivatives.[7,17−20]

To determine the stability of the inhibitor film on the mild steel/solution interface with a longer immersion period, gravimetric measurement was performed at 303 ± 2 K for 12−30 h in 1 M HCl at 50 ppm of CSBs. The results, as

DOI: 10.1021/acsomega.8b00455
ACS Omega 2018, 3, 5654−5668

depicted in Figure 2a, show that with increase in the immersion time the IE remains almost constant up to 30 h.[21]

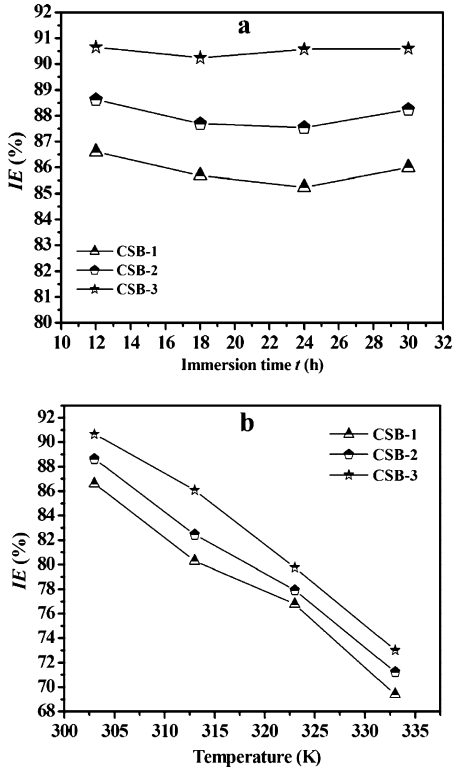

Figure 2. Variation of inhibition efficiency with (a) immersion time and (b) temperature.

2.2.2. Effect of Temperature. The variation of IE of CSBs at the optimum concentration recorded in the temperature range of 303−333 K is shown in Figure 2b. From the figure, it can be seen that the IE of all the three inhibitors slightly decreases with increase in the temperature. It may be attributed to partial desorption of adsorbed inhibitor molecules from the mild steel surface. The effect of temperature on corrosion parameters in the absence and presence of CSBs can be determined by comparison of activation energy (E_a), which is derived with the help of Arrhenius relationship:

$$\log(C_R) = \log A - \frac{E_a}{2.303RT} \quad (1)$$

where A is a constant and T and R are absolute temperature and universal gas constant, respectively. The activation energy (E_a) was calculated from the slope value of the obtained Arrhenius plot in the absence and presence of inhibitors (Figure 3). The calculated values of E_a for blank was 32.96 kJ/mol, while in the presence of CSB-1, CSB-2, and CSB-3, the E_a were 55.18, 58.33, and 62.83 kJ/mol, respectively. The higher activation energy in the presence of CSBs suggests that the CSBs formed a barrier for the dissolution of mild steel in acid solution.

2.2.3. Adsorption Isotherm. To analyze the adsorption behavior of investigated inhibitors on the mild steel surface, several adsorption isotherms were tested including the Langmuir, Temkin, and Frumkin isotherms.[22] Langmuir adsorption isotherm was found to provide the best agreement with the adsorption of used inhibitors on the mild steel surface with a value of regression coefficient (R^2) closer to one, as

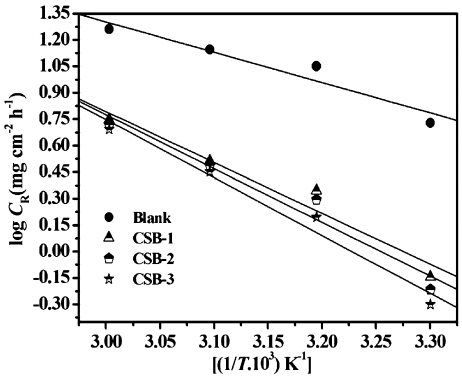

Figure 3. Arrhenius plots for the corrosion rate of mild steel vs the temperature in 1 M HCl.

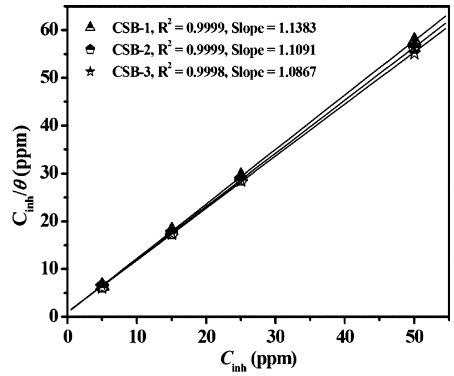

Figure 4. Langmuir isotherm plot for the adsorption of CSBs on mild steel surface in 1 M HCl.

shown in Figure 4, than the Temkin and Frumkin isotherms represented in Figure S2a,b. The Langmuir adsorption isotherm can be represented by the following equation:

$$\frac{C}{\theta} = \frac{1}{K_{ads}} + C \quad (2)$$

where C is the concentration of inhibitor and θ is the fraction of surface coverage which is calculated from the inhibition efficiency. It can be clearly observed from Figure 4 that the plot of C/θ versus C gave the straight line having the slope as unity and the values of R^2 in the order 0.9998−0.9999. The adsorption equilibrium constants (K_{ads}) obtained from the intercept of plot were 1057, 1147, and 1207 L g^{-1} for CSB-1, CSB-2, and CSB-3, respectively, indicating a high adsorption percentage of CSB molecules on the mild steel surface.[23] The K_{ads} is related with adsorption free energy (ΔG^0_{ads}) by the following equation:[24,25]

$$\Delta G^0_{ads} = -RT \ln(1000K_{ads}) \quad (3)$$

The value of 1000 is the concentration of water in acid solution in g L^{-1}. In the present study, the calculated values of ΔG^0_{ads} were −34.95, −35.16, and −35.28 kJ/mol for CSB-1, CSB-2, and CSB-3, respectively. This finding suggested that the CSBs were spontaneously adsorbed on the mild steed surface and exhibited mixed mode of adsorption as discussed previously.[26]

DOI: 10.1021/acsomega.8b00455
ACS Omega 2018, 3, 5654−5668

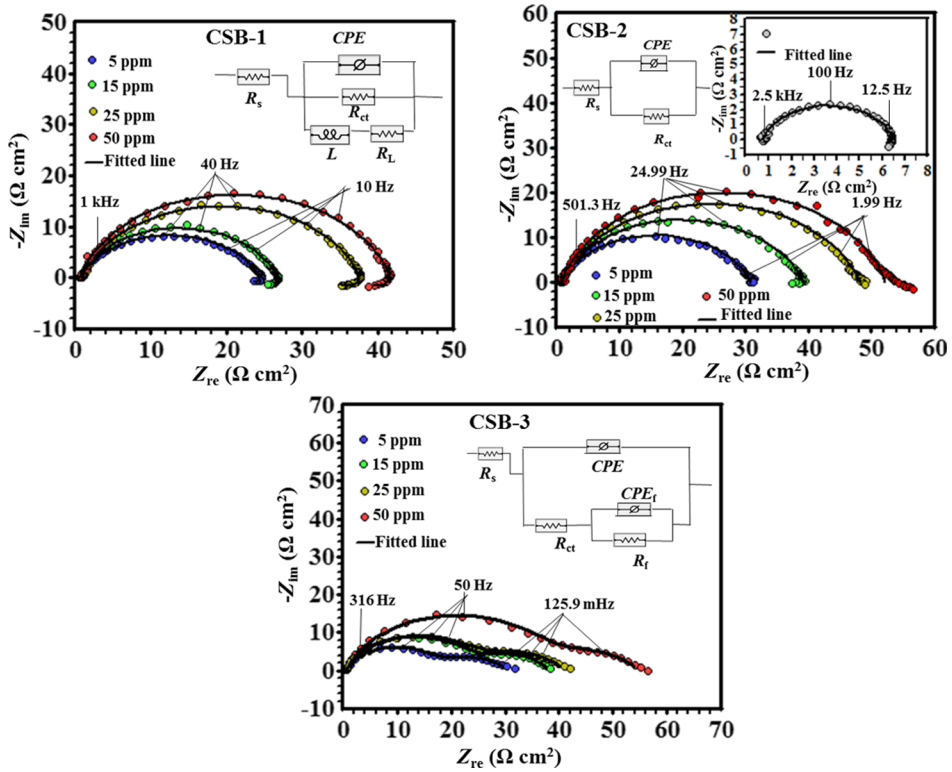

Figure 5. Nyquist plot for mild steel in 1 M HCl without and with different concentrations of CSBs 1 M HCl.

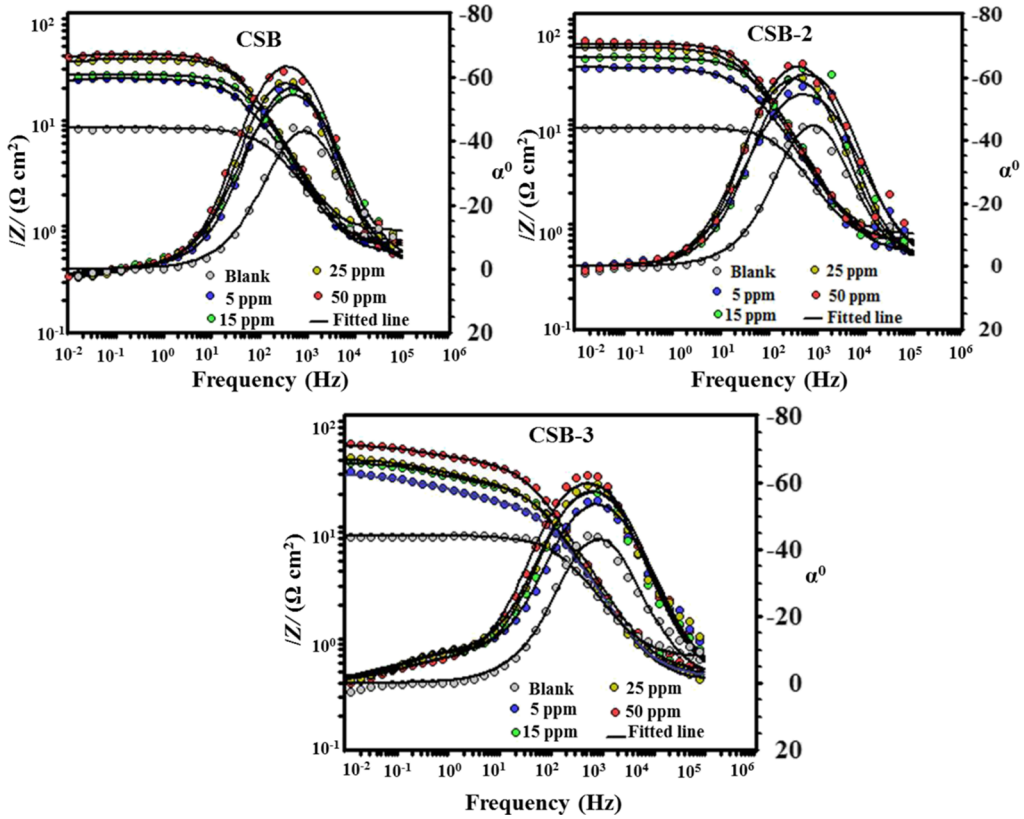

Figure 6. Bode (f vs |Z|) and phase angle (f vs α^0) plots for mild steel in 1 M HCl in the absence and presence of different concentrations of CSBs.

2.3. Electrochemical Study. *2.3.1. Electrochemical Impedance Spectroscopy.* Nyquist and Bode plots of mild steel immersed in 1 M HCl in the absence and presence of CSBs in the concentration range 5−50 ppm are depicted in Figures 5 and 6, respectively. Among the studied CSBs, the Nyquist plots of CSB-1 showed a large capacitive loop at higher frequency (HF) and a small inductive loop at lower frequency (LF). Similar results were observed in previous work.[21,26] The

DOI: 10.1021/acsomega.8b00455
ACS Omega 2018, 3, 5654−5668

Table 2. Electrochemical Impedance Parameters for Mild Steel in 1 M HCl in the Absence and Presence of CSBs at 303 K

inhibitors	concn (ppm)	R_s (Ω cm)	R_L (Ω cm^2)	R_f (Ω cm^2)	R_p (Ω cm^2)	C_{dl} (μF)	C_f (μF)	C (μF)	χ^2	IE (%)
blank		0.727			5.78	278.54			5.36×10^{-3}	
CSB-1	5	0.548	323.3		22.83	161.22			1.34×10^{-3}	74.68
	15	0.719	239.0		25.13	122.10			1.69×10^{-3}	77.00
	25	0.896	383.7		30.99	163.00			1.21×10^{-3}	81.35
	50	0.650	513.4		38.74	129.82			6.70×10^{-3}	85.05
CSB-2	5	0.541			30.30	142.62			4.03×10^{-3}	80.92
	15	0.543			38.13	100.15			7.82×10^{-3}	84.84
	25	0.799			47.54	125.70			2.16×10^{-3}	87.84
	50	0.702			52.02	102.48			6.31×10^{-3}	88.89
CSB-3	5	0.430		12.55	30.55	133.28	24.62	20.78	1.76×10^{-3}	80.08
	15	0.479		14.00	38.63	123.30	17.84	15.58	2.30×10^{-3}	85.04
	25	0.527		17.50	41.53	128.53	14.51	13.04	6.34×10^{-3}	86.08
	50	0.523		15.32	54.91	111.82	24.52	20.11	3.59×10^{-3}	89.47

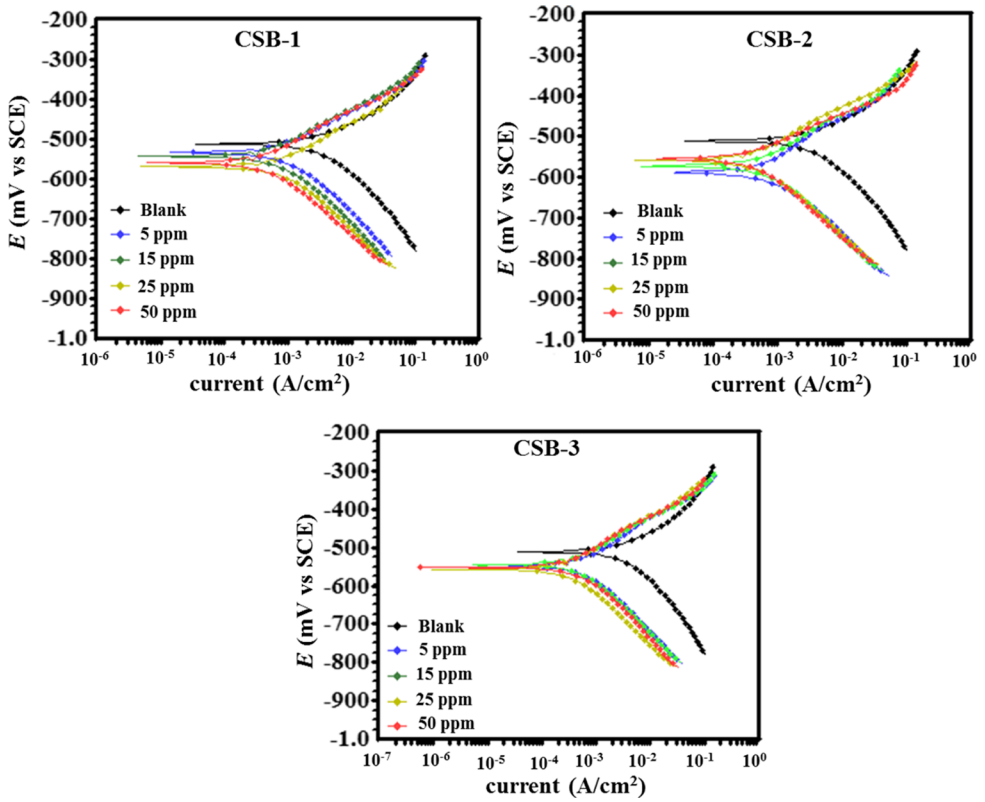

Figure 7. Polarization curves for mild steel in the absence and presence of different concentrations of CSBs in 1 M HCl at 303 K.

occurrence of a capacitive loop at HF indicated that the corrosion of mild steel in 1 M HCl solution is mainly controlled by the charge transfer process,[27] whereas the presence of small inductive loops at LF may be due to the relaxation of adsorbed species or redissolution of the passive layer.[27] The Nyquist plots of CSB-2 showed only one capacitive loop, whereas that of CSB-3 showed two capacitive loops. In case of CSB-3, the occurrence of first time constant at HF corresponding to transfer resistance (R_{ct}) may be ascribed to the charge transfer process between the metal solution interface, and the second capacitive loop is attributable to the film resistance (R_f), arising due to the adsorption of CSB-3 molecules.[28]

To analyze the experimental results, an appropriate equivalent circuit model is required to correctly fit the impedance curves. In the equivalent circuit shown in the inset of Figure 5, L is the inductance and R_s, R_{ct}, R_L, and R_f represent the solution resistance, charge transfer resistance, inductive resistance, and film resistance, respectively. The constant phase elements, CPE and CPE$_f$, are used in the place of double layer capacitance (C_{dl}) and film capacitance (C_f), respectively.[29,30] The impedance of the CPE can be given by

$$Z_{CPE} = Y_0^{-1}(j\omega)^{-n} \quad (4)$$

where Y_0 and n represent the magnitude and exponent (phase shift) of CPE, respectively, and ω_{max} is the angular frequency (given by $\omega = 2\pi f$) at which the imaginary part of impedance is maximum (rad s^{-1}). The double layer capacitance C_{dl} is defined as

$$C_{dl} = Y_0(\omega_{max})^{n-1} \quad (5)$$

DOI: 10.1021/acsomega.8b00455
ACS Omega 2018, 3, 5654−5668

Table 3. Tafel Polarization Parameters for Mild Steel in 1 M HCl Solution in the Absence and at Different Concentrations of CSBs

inhibitors	concn (mM)	E_{corr} (mV/SCE)	β_a (mV/dec)	$-\beta_c$ (mV/dec)	i_{corr} (μA/cm^2)	IE (%)
blank		−511	96.5	149.2	3330	
CSB-1	5	−569	114.3	154.1	953	71.38
	15	−534	101.9	131.7	873	73.78
	25	−542	110.3	129.8	650	80.48
	50	−559	114.8	137.4	513	84.59
CSB-2	5	−589	163.4	128.5	855	74.32
	15	−632	117.7	130.1	632	81.02
	25	−559	114.4	137.0	511	84.65
	50	−555	86.7	133.7	424	87.28
CSB-3	5	−548	116.0	154.7	722	78.32
	15	−544	104.0	134.6	515	84.53
	25	−557	118.1	138.4	383	88.50
	50	−551	90.7	93.8	267	91.98

The same relation is for the film resistance (C_f), hence, in the presence of CSB-3 the corresponding capacitance (C) is as follows[28]

$$C = \frac{C_{dl} \times C_f}{C_f + C_{dl}} \quad (6)$$

In the presence of CSB-1, the ac polarization resistance (R_p) was determined by the following relationship:

$$R_p = R_s + \frac{R_{ct} \times R_L}{R_{ct} + R_L} \quad (7)$$

In case of CSB-2, the R_p is equal to $R_s + R_{ct}$, whereas in case of CSB-3, R_p is equivalent to the $R_s + R_{ct} + R_f$.[31] The IE was calculated from the R_p by using the following equation

$$\text{IE}\ (\%) = \frac{R_p^i - R_p^0}{R_p^i} \times 100 \quad (8)$$

where R_p^0 and R_p^i represent the polarization resistance in the absence and presence of inhibitor, respectively. The obtained impedance results are listed in Table 2. In the case of CSB-1, the value of the R_L was considerably lower than that of the R_p. Hence, for calculating the IE, only the values of R_p were considered.[27] The goodness of fit (χ^2) values were of the order of 10^{-3}, which supported the fitness of the proposed circuit. The results showed that in the presence of CSBs, the values of R_p are increased, indicating the formation of an insulating film between the metal−electrolyte interface, which resists the charge transfer and therefore inhibits the mild steel dissolution. The IE increases with increase in the CSB concentration and reaches a maximum value of 85.05, 88.89, and 89.47% at 50 ppm of CSB-1, CSB-2, and CSB-3, respectively. Hence, among the three CSBs, CSB-3 showed the highest inhibition performance, supporting the gravimetric results. The values of C_{dl} and C are decreased in the presence of inhibitor. According to the Helmholtz model,[27] the drop in C_{dl} may be due to a decrease in the local dielectric constant and/or an increase in the thickness of electrical double layer at the metal solution interface. This indicates that the CSBs (having a lower dielectric constant) adsorb on the metal surface by replacing the pre-adsorbed water having a high dielectric constant and therefore retarding the mild steel corrosion.

The corresponding Bode plots and phase angle plots of CSBs are shown in Figure 6. From Figure 6, the low frequency impedance modulation (f vs $|Z|$) of Bode plots increased with addition of CSBs which further increases with increase in the inhibitor concentration, related to the adsorption of CSBs molecule on the mild steel surface.[32] The value of phase angle increased from 45° to 65° with the addition of CSBs in the concentration range of 5−50 ppm (Figure 6), which indicates an improvement in the inhibition behavior of CSBs with increase in the concentration of the inhibitor molecules.[33]

2.3.2. Potentiodynamic Polarization Study. The potentiodynamic polarization (PDP) curves for mild steel in 1 M HCl in the absence and presence of various concentrations of synthesized CSB inhibitors at 303 K are shown in Figure 7. The values of polarization parameters such as E_{corr}, corrosion current density (i_{corr}), cathodic Tafel slope (β_c), anodic Tafel slope (β_a), and IE are represented in Table 3. It can be observed that with increase in the concentration of CSBs, both the anodic and cathodic current densities are reduced, indicating the suppression of both the anodic Fe dissolution and the cathodic evolution of H_2. In the presence of CSBs, the values of E_{corr} exhibit a pronounced shift toward the cathodic direction, which suggests the cathodic predominance of the inhibitor. This trend confirms a greater influence of the inhibitors on the hydrogen evolution reaction. However, the values of β_c and β_a do not exhibit much change, which indicates that there is no change in the mechanism of hydrogen evolution or Fe dissolution, respectively. The decrease in both the anodic and cathodic currents in the presence of inhibitor without significantly changing the E_{corr} value, suggests that the CSBs exhibit a mixed-type corrosion inhibition behavior. The inhibition efficiency was calculated from the i_{corr} values, through the following relationship:

$$\text{IE}\ (\%) = \frac{i_{corr}^0 - i_{corr}^i}{i_{corr}^0} \times 100 \quad (9)$$

where i_{corr}^0 and i_{corr}^i are the corrosion current densities in the absence and presence of inhibitors, respectively. From the results (Table 3), it is clear that the values of IE increase with increase in the concentration of CSBs and maximum IE were obtained 84.59, 87.28, and 91.98% at 50 ppm of CSB-1, CSB-2, and CSB-3, respectively.

2.4. Surface Study. *2.4.1. FTIR Spectral Analysis.* The FTIR spectra of CSBs, mild steel, and inhibited mild steel after 12 h immersion 1 M HCl solution are shown in Figure 8. The FTIR spectra of the synthesized CSBs are already discussed in section 3 (Figure 1). The FTIR−attenuated total reflectance (ATR) spectra of inhibited mild steel showed corresponding

DOI: 10.1021/acsomega.8b00455
ACS Omega 2018, 3, 5654−5668

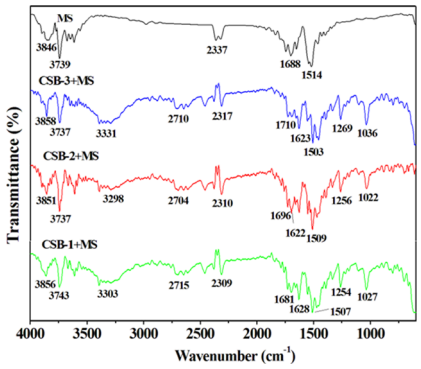

Figure 8. FTIR–ATR spectra of mild steel and adsorbed CSBs on mild steel.

peaks of inhibitors (Figure 8), and these inhibitor peaks are absent in the spectra of the sample without inhibitor, indicating the existence of CSBs on the mild steel surface. The broad peak appeared between 3416 and 3425 cm^{-1} because of the presence of the OH of Schiff bases (Figure 1); these peaks were shifted to 3300–3331 cm^{-1} in inhibited mild steel spectra (Figure 8). This indicates the involvement of the OH group in adsorption.[11] The bands corresponding to C═C (1447–1507 cm^{-1}) and C═N (1647–1598 cm^{-1}) of CSB inhibitors (Figure 1) were slightly shifted to 1503–1509 and 1622–1628 cm^{-1}, respectively, in inhibited spectra of mild steel (Figure 8), which indicated the involvement of the π-bond of imine and benzene ring in the adsorption CSBs on the mild steel surface.[49]

2.4.2. Scanning Electron Microscopy/Energy Dispersive X-ray Analysis (EDX). The scanning electron microscopy (SEM) images of the cleaned and abraded mild steel surface in 1 M HCl in the absence and in the presence of optimum concentrations of CSBs are shown in Figure 9. The image of the blank mild steel sample (i.e., in the absence of inhibitor) depicts considerable damage and surface inhomogeneity because of the corrosive attack of the acid solution. However, in the presence of CSBs, a considerable improvement in the surface smoothness can be easily observed. This is attributable to the adsorption of CSBs over the mild steel surface and the formation of a protective film which isolates the mild steel surface from the surrounding corrosive environment. The EDX spectra of blank (Figure 10) show the presence of oxygen peak is attributed to the slow atmospheric oxidation mild steel surface and therefore the formation of oxide films of Fe, during the analysis. However, in the presence of inhibitors, EDX spectra show the additional peak of nitrogen, indicating the adsorption of CSBs on the mild steel surface.

2.5. Theoretical Studies. *2.5.1. Quantum Chemical Parameters.* The optimized molecular structures and the corresponding frontier molecular orbital electron density of neutral CSBs in aqueous phase are shown in Figure 10. The highest occupied molecular orbital (HOMO) electron density provides information about the sites of the molecule that are more likely to donate electrons to the appropriate orbital of an acceptor molecule. The lowest unoccupied molecular orbital (LUMO) electron density shows the sites that are more likely to accept electrons from a suitable donor species. The energy of the HOMO (E_{HOMO}) is associated with the tendency of electron donation, whereas the energy of the LUMO (E_{LUMO}) is associated with the tendency of electron acceptance. Therefore, a higher value of E_{HOMO} signifies an easier donation

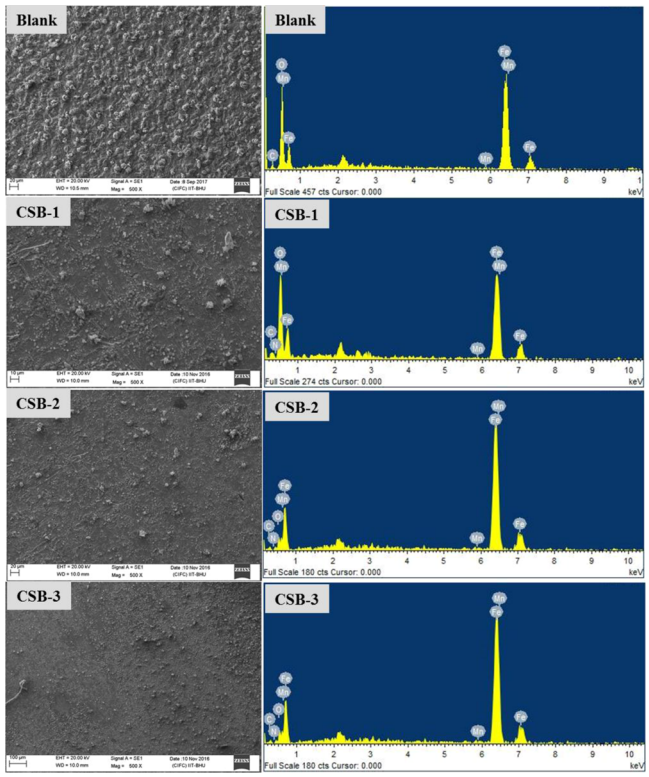

Figure 9. SEM and EDX images of mild steel: in the absence of CSBs (blank) and in the presence of 50 ppm of CSB-1, CSB-2, and CSB-3.

of electrons from the inhibitor to the vacant d-orbitals of the metal. On the other hand, a lower value of E_{LUMO} suggests an easier tendency of the inhibitor to accept electrons from the filled orbitals of metal via retro-donation. The calculated quantum chemical parameters of the three CSBs are listed in Table 4 along with the experimentally obtained corrosion inhibition efficiency values.

Following Koopman's theorem, the frontier orbital energies can be given by

$$-E_{HOMO} = I \tag{10}$$

$$-E_{LUMO} = A \tag{11}$$

where I and A represent the ionization potential and electron affinity of the molecule, respectively. Thus, a higher value of E_{HOMO} in CSB 2 than CSB 1 is attributed to the presence of the dimethyl amino group. The −OH and $-OCH_3$ groups of CSB-3 contribute toward further increase in the E_{HOMO} values. This observation suggests that CSB 3 exhibits the highest electron donation tendency. The E_{LUMO} on the other hand presents an inverse trend, that is, the CSB 1 shows the highest tendency to accept electrons. However, the ΔE value, which is a measure of the reactivity index, is the lowest in the case of CSB-3. This further supports its higher tendency to adsorb on the metal surface.

The absolute electronegativity (χ) defines the electron attraction ability of a group of atoms toward itself and it can be given as

$$-\mu = \chi = \frac{1}{2}(I + A) = -\frac{1}{2}(E_{LUMO} + E_{HOMO}) \tag{12}$$

According to HSAB principle,[50] the electron transfer takes place from the region of lower electronegativity to the region of

DOI: 10.1021/acsomega.8b00455
ACS Omega 2018, 3, 5654–5668

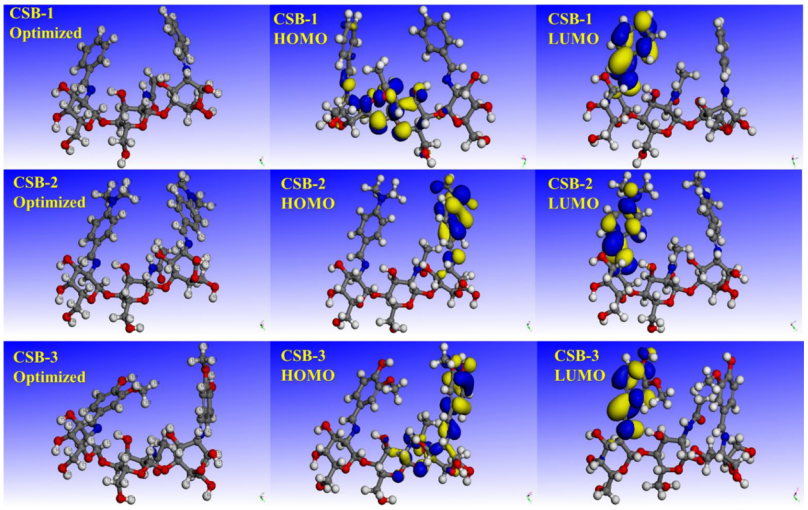

Figure 10. HOMOs, LUMOs, and molecular electrostatic potential of protonated CSB inhibitors in aqueous phase.

Table 4. Quantum Chemical Parameters

	parameters									
inhibitors	E_{HOMO} (eV)	E_{LUMO} (eV)	ΔE (eV)	η (eV)	σ (eV)	χ (eV)	IE	EA	ΔN_{110}	IE (%)
CSB-1	−5.462	−2.188	3.274	1.637	0.611	3.825	5.462	2.188	0.304	88.63
CSB-2	−4.835	−1.754	3.081	1.540	0.649	3.294	4.835	1.754	0.495	89.87
CSB-3	−4.452	−1.763	2.689	1.344	0.744	3.107	4.452	1.763	0.637	91.47

higher electronegativity until the chemical potentials (μ) become equal. The global hardness (η) poses a barrier which needs to be over for the electron transfer to take place. In other words, a higher value of η signifies the lesser tendency of electron transfer. Its inverse, the global softness (σ), on the other hand, presents the higher tendency of a molecule to undergo chemical reaction. Pearson has postulated that the hard molecules have a large HOMO−LUMO gap and soft molecules have a small HOMO−LUMO gap.[34] Therefore, the energy gap ΔE can be directly related to the global hardness. This relationship is based on the principle of maximum hardness, which states that "a molecule arranges itself to be as hard as possible."

The global hardness and softness can be related to the energy of HOMO and LUMO as follows:

$$\eta = \frac{1}{2}(I - A) = -\frac{1}{2}(E_{HOMO} - E_{LUMO}) \quad (13)$$

$$\sigma = \frac{1}{\eta} \quad (14)$$

From Table 4, it is obvious that the CSB 3 has the lowest values of χ, which suggests the highest tendency of electron donation. Also, the lowest η and consequently the highest σ values suggest the highest reactivity of CSB-3. Thus, these data correlate well with those of the trend in the energy gap values shown above. Pearson has reported that the fraction of electrons transferred between inhibitor molecules and the metal surface can be estimated according to the following equation:

$$\Delta N = \frac{\chi_{metal} - \chi_{inh}}{2(\eta_{metal} + \eta_{inh})} \quad (15)$$

where χ_{metal} and χ_{inh} represent the absolute electronegativities of the metal and inhibitor, respectively, and χ_{metal} and χ_{inh} denote the global hardness values of the metal and inhibitor, respectively. Here, it is important to mention that the value ΔN does not provide the exact number of electrons transferred between the inhibitor and the metal surface. It is indicative of the electron donating ability or a tendency to donate electrons. To calculate the fraction of electrons transferred between the inhibitor and the metal, a theoretical value of 7 eV for χ_{Fe} of bulk iron and a global hardness $\eta_{Fe} = 0$ are used, assuming $I = A$ for bulk metal.[35]

Kokalj[36] has reported that the use of work function metal rather than χ_{Fe} is more suitable for an adsorbate−metal surface interaction. Thus, using it in the place of χ_{Fe} and putting η_{Fe} = 0, the above equation becomes 15

$$\Delta N = \frac{\phi_{Fe} - \chi_{inh}}{2\eta_{inh}} \quad (16)$$

The DFT calculated values for Fe(100), Fe(110), and Fe(111) surfaces are 3.91, 4.82, and 3.88 eV, respectively. In the present investigation, we have considered the Fe(110) surface because of its higher stabilization energy and packed surface. The transfer of electrons from the inhibitor molecule to the metallic surface will take place when $\Delta N > 0$ and vice versa.[21] From the data shown in Table 4, it is clear that (i) for the three CSBs, $\Delta N > 0$ and (ii) the CSB 3 shows the highest value of ΔN. Therefore, it is clear that the trend of calculated quantum chemical parameters matches the trend of experimentally determined corrosion inhibition efficiency.

2.5.2. Fukui Index Analysis. An analysis of Fukui indices was performed to theoretically determine the sites present in the inhibitor molecules that are more likely to participate in the donor−acceptor type interaction with the metal surface. The sites on the inhibitor molecules that donate and accept electrons are represented by f_k^+ (nucleophilic site) and f_k^- (electrophilic site), respectively. A higher value of the f_k^- and

DOI: 10.1021/acsomega.8b00455
ACS Omega 2018, 3, 5654−5668

Table 5. Fukui Indices of Reactive Sites on CSB Molecules

CSB-1				CSB-2				CSB-3			
atom	F^+	F^-	Mulliken charge	atom	F^+	F^-	Mulliken charge	atom	F^+	F^-	Mulliken charge
C(1)	0.004	0.016	0.141	C(1)	−0.002	0.001	0.152	C(1)	0.002	−0.010	0.154
C(2)	0.000	0.003	0.209	C(2)	0.002	−0.005	0.198	C(2)	−0.005	−0.005	0.193
C(3)	0.000	0.003	−0.029	C(3)	−0.003	−0.006	−0.024	C(3)	−0.012	−0.010	−0.022
C(4)	0.002	0.001	0.455	C(4)	0.002	−0.003	0.455	C(4)	−0.001	−0.003	0.458
O(5)	0.001	0.014	−0.558	O(5)	−0.003	0.008	−0.558	O(5)	0.009	0.016	−0.526
C(6)	0.001	0.004	0.186	C(6)	−0.001	−0.002	0.168	C(6)	−0.005	−0.006	0.168
O(7)	0.000	0.007	−0.514	O(7)	0.001	0.003	−0.517	O(7)	0.004	0.010	−0.482
C(8)	0.003	0.002	0.135	C(8)	0.009	−0.008	0.146	C(8)	0.005	0.002	0.130
O(9)	0.001	0.004	−0.552	O(9)	−0.001	0.003	−0.557	O(9)	0.007	0.012	−0.499
N(10)	0.006	0.011	−0.321	N(10)	−0.003	**0.042**	−0.353	N(10)	0.035	0.020	−0.307
C(11)	0.002	0.013	0.114	C(11)	0.001	0.017	0.108	C(11)	0.033	0.003	0.114
C(12)	0.000	0.004	0.041	C(12)	−0.004	**0.048**	0.012	C(12)	0.001	0.016	0.040
C(13)	0.001	0.005	−0.076	C(13)	−0.001	0.017	−0.074	C(13)	0.018	0.013	−0.079
C(14)	0.001	0.005	−0.052	C(14)	−0.000	0.046	−0.110	C(14)	0.004	0.012	−0.085
C(15)	0.000	0.013	−0.061	C(15)	0.000	0.021	0.241	C(15)	0.023	0.023	0.262
C(16)	0.001	0.004	−0.058	C(16)	0.003	**0.054**	−0.128	C(16)	0.009	0.027	0.282
C(17)	0.001	0.009	−0.070	C(17)	0.002	0.022	−0.071	C(17)	0.010	0.010	−0.136
O(18)	0.001	0.028	−0.521	O(18)	−0.004	0.007	−0.516	O(18)	−0.006	0.006	−0.495
O(19)	0.003	**0.107**	−0.542	O(19)	−0.000	0.005	−0.546	O(19)	0.006	**0.048**	−0.511
C(20)	0.000	0.006	0.437	C(20)	−0.003	0.001	0.448	C(20)	0.003	−0.008	0.447
C(21)	0.000	0.015	0.049	C(21)	0.006	−0.007	0.044	C(21)	−0.002	−0.009	0.048
C(22)	0.010	0.003	0.166	C(22)	−0.015	0.003	0.169	C(22)	−0.012	−0.000	0.164
C(23)	0.003	0.002	0.193	C(23)	0.000	−0.001	0.193	C(23)	−0.002	0.002	0.194
C(24)	0.005	0.015	0.135	C(24)	−0.000	−0.002	0.128	C(24)	−0.005	−0.012	0.135
O(25)	0.001	**0.092**	−0.537	O(25)	0.005	−0.001	−0.545	O(25)	0.009	0.027	−0.522
C(26)	0.000	0.001	0.154	C(26)	0.000	0.000	0.166	C(26)	−0.000	−0.005	0.175
O(27)	0.001	0.009	−0.551	O(27)	0.001	0.001	−0.558	O(27)	0.007	0.013	−0.510
N(28)	0.002	0.033	−0.371	N(28)	−0.007	0.003	−0.362	N(28)	−0.001	0.017	−0.392
C(29)	0.002	0.018	0.456	C(29)	0.001	0.002	0.452	C(29)	−0.004	0.007	0.449
O(30)	0.007	**0.062**	−0.559	O(30)	0.006	−0.001	−0.570	O(30)	0.017	**0.046**	−0.473
C(31)	0.011	0.009	−0.229	C(31)	−0.016	0.013	−0.227	C(31)	−0.005	−0.001	−0.212
O(32)	0.009	0.022	−0.578	O(32)	0.010	−0.001	−0.583	O(32)	0.001	0.004	−0.569
O(33)	0.005	0.014	−0.543	O(33)	0.003	0.002	−0.544	O(33)	−0.000	0.007	−0.509
C(34)	0.005	0.007	0.420	C(34)	−0.004	−0.001	0.420	C(34)	0.001	−0.001	0.430
C(35)	0.025	0.002	0.032	C(35)	−0.028	−0.002	0.036	C(35)	−0.022	−0.006	0.034
C(36)	0.006	0.001	0.207	C(36)	−0.003	−0.002	0.206	C(36)	−0.008	−0.001	0.215
C(37)	0.002	0.003	0.179	C(37)	0.002	−0.002	0.181	C(37)	0.000	−0.002	0.184
C(38)	0.011	0.004	0.140	C(38)	−0.010	0.006	0.137	C(38)	−0.009	−0.006	0.143
O(39)	0.008	0.004	−0.532	O(39)	0.007	0.001	−0.532	O(39)	0.008	0.004	−0.521
C(40)	0.001	0.002	0.161	C(40)	0.002	−0.002	0.165	C(40)	−0.003	−0.002	0.171
O(41)	0.003	0.000	−0.559	O(41)	0.001	0.001	−0.559	O(41)	0.008	0.007	−0.522
N(42)	**0.094**	0.004	−0.406	N(42)	**0.089**	0.012	−0.438	N(42)	**0.065**	0.005	−0.404
C(43)	**0.133**	0.004	0.137	C(43)	**0.135**	0.007	0.125	C(43)	**0.065**	0.002	0.151
C(44)	0.017	0.001	0.035	C(44)	0.003	0.016	0.001	C(44)	−0.000	0.008	0.038
C(45)	**0.070**	0.001	−0.078	C(45)	**0.075**	0.005	−-0.081	C(45)	**0.040**	0.001	−0.143
C(46)	0.023	0.001	−0.054	C(46)	0.022	0.016	−0.118	C(46)	0.011	0.010	0.290
C(47)	**0.090**	0.004	−0.066	C(47)	**0.069**	0.008	0.238	C(47)	**0.045**	0.010	0.263
C(48)	0.031	0.002	−0.059	C(48)	0.027	0.017	−0.128	C(48)	0.015	0.009	−0.091
C(49)	**0.058**	0.002	−0.071	C(49)	**0.054**	0.007	−0.072	C(49)	0.021	0.009	−0.067
O(50)	0.011	0.004	−0.542	O(50)	0.008	0.004	−0.545	O(50)	0.002	0.006	−0.503
O(51)	0.002	0.008	−0.561	O(51)	−0.003	0.008	−0.563	O(51)	0.003	0.004	−0.531
	TNC: −9.65			N(64)	0.000	0.075	**−0.442**	O(64)	0.023	**0.049**	−0.437
				N(92)	0.022	0.025	−0.437	O(65)	0.007	0.023	−0.537
				C(97)	−0.001	−0.012	−0.002	O(91)	0.014	0.008	−0.539
				C(98)	−0.000	−0.014	0.000	O(92)	**0.041**	0.027	−0.437
				C(99)	−0.011	−0.004	0.002	C(97)	−0.010	−0.015	0.117
				C(100)	−0.012	−0.003	−0.004	C(98)	−0.014	−0.001	0.099
					TNC: −10.764				**TNC: −11.061**		

DOI: 10.1021/acsomega.8b00455
ACS Omega 2018, 3, 5654−5668

f_k^+ parameter represents a greater tendency of electron donation and acceptance, respectively. The calculated Fukui index values are listed in Table 5. It can be observed that the sites most susceptible for electron donation in CSB-1 are O(19), O(25), and O(30), whereas the sites most susceptible for electron acceptance are N(42), C(43), C(45), C(47), and C(49). In CSB-2, the sites susceptible for electron donation are N(10), C(12), C(16), and N(64), whereas the sites susceptible for electron acceptance are N(42), C(43), C(45), C(47) and C(49). In case of CSB-3, the susceptible sites for electron donation are O(19), O(30), and O(64), whereas the susceptible sites for electron acceptance are N(42), C(43), C(45), and O(92). Therefore, it can be observed that in the CSBs, the phenyl rings and the functional groups are the most active sites for the electron donation−acceptance type interaction, and hence, these are the sites most likely to facilitate adsorption over the mild steel surface.

2.5.3. MD Simulation. The effective corrosion inhibitors exert their function by either acquiring a specific molecular structure, which contains diverse reactive sites and/or by adapting their conformation in more planar form covering a large area of the corroded surface.[37] Both modes of action increase the ability of the inhibitor molecules to interact with the surface of the metal. Therefore, a full understanding of a corrosion inhibitor function requires an interpretable description of complex interactions between an inhibitor and metal atoms. MD simulations have been largely used to study the corrosion inhibition process in solvent allowing us to examine inhibition mechanisms and inhibitor conformation change in atomistic detail. In the current study, MD simulation was performed for the three CSBs using Discover module implemented in Materials Studio software. All simulation systems reach equilibrium only if both the energy and temperature reach balance.[38,39] Figure 11 shows the equilibrium configurations of the surface adsorbed inhibitor molecules. As can be seen from Figure 11, the inhibitor molecules adsorbed on the iron surface in a parallel manner which can help ensure coverage of a maximum surface area of the corroded metal. Polymer-based inhibitors are thought to have higher affinities for the metal surface than small molecule inhibitors, because they can interact with a larger contact area compared with small molecules. In this situation, strong interactions between inhibitor molecules and iron atoms can be produced. The presence of several reactive sites such as nonbonding electrons present on nitrogen atoms of the inhibitor molecules and methoxy and hydroxy groups enhance the tendency of said compounds to donate their electrons to the vacant d-orbitals of iron atoms.[40] In fact, perhaps the most striking picture to emerge from the data shown in Figure 11 is the adsorption profile of CSB-3; it is observed that the phenyl ring containing methoxy and hydroxy groups exists in close contact with the iron surface. Even though the changes between inhibitor molecules were small from a molecular point of view, the presence of both groups in CSB-3 was most significant among other groups. Thus, a change in the structure, and/or in the nature of the functional group, is expected to affect the compound's efficiency, as observed in this study. Generally speaking, the compounds having the $-N(CH_3)_2$ group have high inhibitive activity as compared to the compounds having $-OCH_3$ and $-OH$ groups.[40] However, in the present study, the presence of both groups ($-OCH_3$ and $-OH$) in the parent structure increases the electron donating tendency of CSB-3 as compared to CSB-1 and CSB-2, leading to more impact on corrosion retardation ability. Lesser inhibition shown by the CSB-2 as compared to CSB-3 may be attributed to the orientation of substituent $-N(CH_3)_2$ group, which prevents its flat orientation on the metal surface causing less adsorption and thereby less inhibition. A similar explanation has been given earlier.[41]

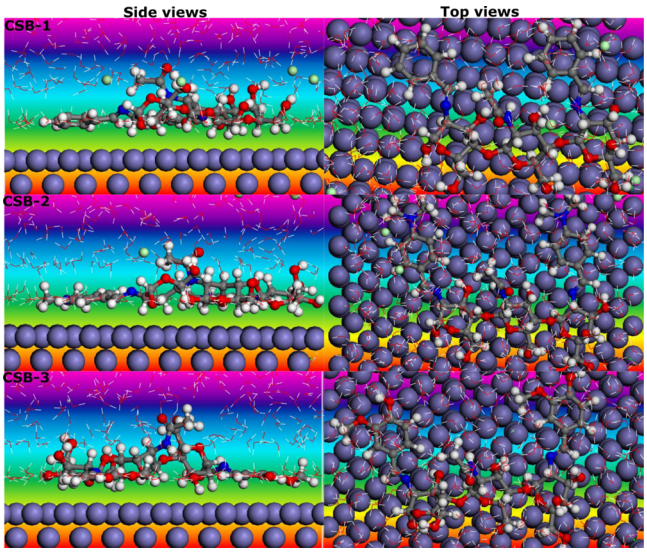

Figure 11. Side and top views of the final adsorption of tested inhibitors on the Fe(110) surface in solution.

Table 6 shows the binding ($E_{binding}$) and interaction ($E_{interaction}$) energies of three inhibitors obtained under equilibrium conditions. Closer inspection of the table shows that all the tested compounds are associated with strong, stable, and spontaneous adsorption on the Fe(110) surface.[42,43] The high magnitude of the binding energies for all the inhibitor molecules indicates that they adsorbed through more than one adsorption centers.[44,45] A detailed analysis of the results showed that the magnitude of interaction energy increases on going from CSB-1 to CSB-3, which directly indicates that effectiveness of the adsorption and thereby inhibition efficiency increase in the same sequence. The results of the study also indicate that CSB-1 and CSB-2 have significantly less interaction energy than CSB-3, although in contrast, no difference was observed in the adsorption profile of the three compounds. These findings provide further evidence for a strong association between functional groups, heteroatoms, and inhibitive performances. The compound with both hydroxy and methoxy groups in its molecular structure appears to have a marked influence on the corrosion inhibition process as compared to other groups.

Table 6. Selected Energy Parameters Obtained from MD Simulations for Adsorption of Inhibitors on the Fe(110) Surface

system	$E_{interaction}$ (kJ/mol)	$E_{binding}$ (kJ/mol)
Fe(110)/CSB-3	−666.18	666.18
Fe(110)/CSB-2	−633.39	633.39
Fe(110)/CSB-1	−509.11	509.11

2.5.4. Radial Distribution Function. After showing the adsorption potentialities of the studied corrosion inhibitors, we would like to discuss the molecule−molecule interaction types

DOI: 10.1021/acsomega.8b00455
ACS Omega 2018, 3, 5654−5668

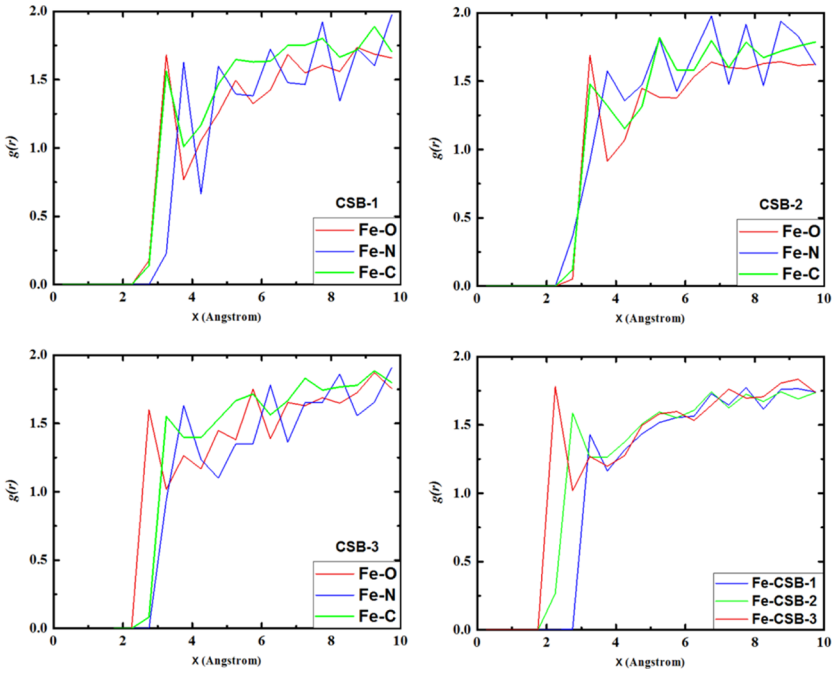

Figure 12. RDFs of tested inhibitors adsorbed on the Fe(110) surface in solution.

by measuring the typical bonding length. For this purpose, radial distribution function (RDF) was calculated for the three inhibitors using MD simulations trajectories. Particularly, the typical bond lengths of physisorption are greater than 3.5 Å, much longer than chemical interaction types, which fall in the range of 1−3.5 Å.[46]

RDFs of all inhibitor molecules are represented in Figure 12. It is well-known that the position of a first prominent peak in the RDF curve can reflect the state of inhibitor molecules adjacent to the iron surface.[8] On the basis of the radial distribution of inhibitor molecules, a first prominent peak for (CSB-3)−Fe, (CSB-2)−Fe, and (CSB-1)−Fe are observed, located at 2.25, 2.75, and 3.25 Å, respectively, which are all less than 3.5 Å, signifying the most important interactions of all inhibitor atoms with the iron surface. To gain further understanding of potential atomic sites that may underlie the effectiveness of the tested compounds, we analyzed the impact of the oxygen, nitrogen, and carbon atoms on the metal−inhibitor interaction. According to the profiles of RDFs in Figure 12, it can be seen that generally all atoms have significant interactions with the metal surface. The most important RDF is calculated for oxygen atoms, which have the peak distance lower than 3.5 Å in all inhibitor molecules. The fact that oxygen atoms have very pronounced interactions with the metal surface could be very important because these atoms are located in the near vicinity of the iron atoms, meaning that the inhibitor−iron interactions could be of importance. Carbon atoms have the peak distances located at around 3.5 Å, indicating that π-electrons contribute effectively to the interaction between organic species and the iron surface. On the other side, nitrogen atoms have the peak distances higher than 3.5 Å, meaning the ability of these atomic sites to be protonated in the studied medium, and therefore, a physical interaction can be easily created.[24] Theoretical simulations and experimental results support the assumption that including two electron donating groups in the parent structure will optimize the corrosion inhibition performances of our compounds.

3. CONCLUSIONS

In the present study, three CSBs were synthesized and investigated as corrosion inhibitors for mild steel in 1 M HCl solution by the experimental and theoretical methods. On the basis of results, following conclusions have been drawn:

1. The inhibition efficacy increases with increasing the inhibitor concentration and maximum inhibition efficiency was obtained 84.59, 87.28 and 91.89% for CSB-1, CSB-2, and CSB-3, respectively, at 50 ppm.
2. The adsorption of CSB inhibitors on the mild steel surface obeys the Langmuir adsorption isotherm. The values of ΔG^0_{ads} (−34.95 to −35.28 kJ/mol) indicates that the adsorption of inhibitors on the mild steel surface is spontaneous and takes place by mixed mode of adsorption.
3. The electrochemical impedance spectroscopy (EIS) results suggested that CSBs protect the mild steel corrosion by the formation of a protective inhibitor film at the metal−electrolyte interface.
4. The PDP results reveal that all the three CSBs behave as mixed-type corrosion inhibitors and exhibit cathodic predominance.
5. The formation of the inhibitor film was corroborated by FTIR−ATR and SEM/EDX.
6. The theoretical studies via DFT, Fukui indices, and MD further supported the experimental results.

4. EXPERIMENTAL SECTION

4.1. Materials and Test Solution. Chitosan was purchased from Sigma-Aldrich. The aldehydes were obtained from Avra. The corrosion tests were performed on the mild steel coupons having weight percentage composition (wt %) of C; 0.0737%, Si; 0.0826%, Mn; 0.556%, P; 0.0304%, S; 0.0141%, and balance Fe (99.2432%). The mild steel coupons were cut in dimension 2.5 cm × 2.0 cm × 0.05 cm were taken for the gravimetric study and surface analysis. For the electrochemical tests, the mild

DOI: 10.1021/acsomega.8b00455
ACS Omega 2018, 3, 5654−5668

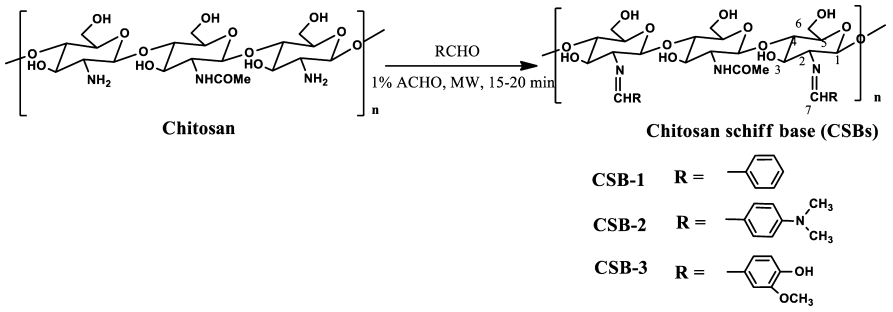

Figure 13. Synthetic scheme of CSBs.

steel specimens of dimension 8.0 cm × 1.0 cm × 0.05 cm were taken, having 1 cm^2 exposed area, and the rest of the surface was covered by epoxy resin. Prior to conducting the experiment, the mild steel specimens were mechanically polished using different grades of SiC emery papers (from 600 to 1200), then degreased with acetone, washed with double distilled water, dried, and stored in a desiccator before use.

The test solution of 1 M HCl was prepared from analytical grade hydrochloric acid (HCl. 37% Fisher Scientific) with double distilled water. The tests were carried out in aerated and unstirred solution at 303 ± 2 K.

4.2. Synthesis of Inhibitors (CSBs). The Schiff bases of chitosan (CS) were synthesized according to Figure 13. CS (3 g) was added to 99 mL distilled water and was dissolved by addition of 1 g glacial acetic acid at room temperature. The 0.05 mol of different aldehydes (benzaldehyde, 4-dimethylamino-benzaldehyde, and 4-hydroxy-3-methoxybenzaldehyde) was dissolved in 95% ethanol. This solution was added to the flask containing chitosan solution dropwise with constant stirring at 303 K for 30 min. The mixture was subjected to irradiation in a Microwave Synthesis Workstation (Sineo MAS-II: Shanghai, China), which is capable to deliver selectable power up to 1000 W at a frequency of 2450 MHz at full power. The reactor system was equipped with an infrared temperature measurement tube, a mechanical agitator, and a 100 mL reaction flask coupled to a reflux condenser. The power was set at 600 W, and the sample temperature was ramped to 60 °C and kept at 60 °C for 15−20 min. The resulting yellow gel solution of Schiff base was precipitated using acetone followed by several acetone washing steps to remove any unreacted aldehyde. Subsequently, the samples were dried under vacuum at 303 K and the purity was tested by thin-layer chromatography (90% *n*-hexane−ethyl acetate). The FTIR spectra were recorded by using an FTIR (PerkinElmer Version 10.03.05 instrument) spectrometer, and ^{1}H NMR spectra were recorded using a Bruker 500 MHz instrument operating at 500 MHz.

4.3. Corrosion Tests. *4.3.1. Gravimetric Study.* Gravimetric tests were performed through the immersion of precleaned mild steel specimen in a conical flask containing 100 mL test solution (1 M HCl and 1 M HCl with different concentrations of CSBs) at 303 ± 2 K in the thermostat, by using the ASTM procedure.[47] The mild steel specimens were taken out after 6 h, washed with water and acetone, dried, and reweighed for the calculation of weight loss. Each experiment was repeated twice, and the average weight loss values were used to calculate the corrosion rate C_R (mg cm^{-2} h^{-1}) by using the following equation[48]

$$C_R = \frac{w}{At} \tag{17}$$

where w is the average weight loss (mg), A is the area of specimen (cm^{-2}), and t is the exposure time (h^{-1}). By using the calculated values of C_R, inhibition efficiency (IE %) and surface coverage (θ) can be calculated through the following relationship[49]

$$\text{IE}\ (\%) = \frac{C_R - C_{R(i)}}{C_R} \times 100 \tag{18}$$

$$\theta = \frac{C_R - C_{R(i)}}{C_R} \tag{19}$$

where C_R and $C_{R(i)}$ are the obtained corrosion rates in the absence and presence of CSBs, respectively.

4.3.2. Electrochemical Tests. The electrochemical experiments were performed using a Gamry Potentiostat/Galvanostat (model G-300), and the obtained data were fitted and analyzed by a Gamry Echem Analyst 5.0 software. A three electrode glass cell assembly was used for conducting the electrochemical experiments, which consisted of a mild steel coupon having 1 cm^2 exposed area (one sided) as the working electrode, graphite rod as the counter electrode, and saturated calomel electrode (SCE) as the reference electrode.

Prior to each experiment, the working electrode was immersed in the test solution for 30 min to achieve a steady state open circuit potential (E_{OCP}). The EIS was conducted on mild steel at E_{OCP} in the frequency range 100 kHz to 0.01 Hz by applying the ac signal 10 mV peak to peak. Finally, the PDP experiment was carried out by changing the potential in the range from −250 to +250 mV versus E_{OCP} with a constant sweep rate of 0.1 mV/s.

4.3.3. Surface Study (FTIR and SEM/EDX). FTIR was used to confirm the adsorption of CSBs on the metal surface using the ATR technique. The surface morphology and elemental composition of uninhibited and inhibited mild steel specimens was studied using the SEM/EDX, Zeiss EVO 50 XVP instrument. The SEM images of mild steel were recorded at 500× magnification.

4.4. Theoretical Study. *4.4.1. Quantum Chemical Calculations.* The quantum-based calculations were conducted using Materials Studio software package (version 6.0)[50] at DFT/GGA level using BOP functional and DNP basis set on all atoms.[48,51,52] The calculations were carried out after optimizing the structures. The COSMO[53] controls were used for solvation effects (aqueous phase).

4.4.2. Fukui Functions. The calculation of the Fukui functions was carried out using UCA-FUKUI v 1.0 software[54] using the output file from Gaussian 09. The Fukui function (f_k)

DOI: 10.1021/acsomega.8b00455
ACS Omega 2018, 3, 5654−5668

is the first derivative of the electron density $\rho(\vec{r})$ with respect to the number of electrons N in a constant external potential $\nu(\vec{r})$ and can be expressed as follows

$$f_k = f_k = \left(\frac{\partial\rho(\vec{r})}{\partial N}\right)_{\nu(\vec{r})} \quad (20)$$

The nucleophilic and electrophilic attacks were computed using the finite-difference approximations method[55]

$$f_k^+ = q_k(N+1) - q_k(N) \text{ (for nucleophilic attack)} \quad (21)$$

$$f_k^- = q_k(N) - q_k(N-1) \text{ (for electrophilic attack)} \quad (22)$$

Here, q_k represents the gross charge on the atom. The charges on the anionic, neutral, and cationic species are denoted by $q_k(N+1)$, $q_k(N)$, and $q_k(N-1)$, respectively.

4.4.3. MD Simulation and RDF. MD simulation is currently the most popular method for investigating the intermolecular interactions between corrosion inhibitor molecules and the metal surface under periodic boundary situations.[56,57] In the present study, the Fe(110) surface with a slab of 5 Å was chosen for MD simulation as this iron surface is associated with high stabilization energy with highly packed structure. To provide a larger surface area for metal−inhibitor interactions, the simulations were carried out in a simulation box (24.82 × 24.82 × 35.69 Å^3), which included $9Cl^-$, $491H_2O$, $9H_3O^+$, and one inhibitor molecule. The simulations were constructed with the help of the Visualizer, Amorphous Cell, and Discover modules implemented in BIOVIA Materials Studio commercial software.[50] MD simulations are performed at temperatures T = 303 K maintained constant by the Andersen thermostat, at a time step of 0.1 fs, NVT (fixed atom number, system volume, and temperature) ensemble and a simulation time of 2000 ps to reach simulation system under an equilibrium state. The energy minimization and MD calculation processes were performed using COMPASS (the condensed-phase optimized molecular potential for atomistic simulation studies) force field.[58] The extent of the interactions of the inhibitor molecules adsorbed on the Fe(110) surface can be demonstrated by their interaction ($E_{interaction}$) and binding ($E_{binding}$) energies derived using eqs 23 and 24.[37]

$$E_{interaction} = E_{total} - (E_{surface+solution} + E_{inhibitor}) \quad (23)$$

$$E_{binding} = -E_{interaction} \quad (24)$$

where E_{total} represents the energy of the entire system, $E_{surface+solution}$ denotes the entire energy of Fe(110) and electrolytic solution in the absence of inhibitor molecules, and $E_{inhibitor}$ denotes the whole energy of inhibitor molecules.

For more detailed information about the interactions between the inhibitor molecules and metal surface, RDFs (defined here as the probability of finding particle B within the range around particle A) were calculated from the simulation trajectories:[59] the RDF is defined by Hansen and McDonald as[60]

$$g_{AB}(r) = \frac{1}{\langle\rho_B\rangle_{local}} \times \frac{1}{N_A}\sum_{i\in A}^{N_A}\sum_{j\in B}^{N_B}\frac{\delta(r_{ij}-r)}{4\pi r^2} \quad (25)$$

where local represents the particle density of B averaged over all shells around particle A.

■ ASSOCIATED CONTENT

Supporting Information

The Supporting Information is available free of charge on the ACS Publications website at DOI: 10.1021/acsomega.8b00455.

^{1}H NMR spectra of chitosan, CSB-1, CSB-2, and CSB-3 and Temkin and Fremkin adsorption isotherm plots for the adsorption of CSBs on the mild steel surface in 1 M HCl (PDF)

■ AUTHOR INFORMATION

Corresponding Authors

*E-mail: maquraishi.apc@itbhu.ac.in. Phone: +966538600057 (M.A.Q.).

*E-mail: vsrivastava.apc@iitbhu.ac.in (V.S.).

ORCID

Mumtaz A. Quraishi: 0000-0002-7822-0084

Notes

The authors declare no competing financial interest.

■ ACKNOWLEDGMENTS

J.H. gratefully acknowledges the Senior Research Fellowship from MHRD, New Delhi, India.

■ REFERENCES

(1) Martins, A. F.; Facchi, S. P.; Follmann, H. D. M.; Pereira, A. G. B.; Rubira, A. F.; Muniz, E. C. Antimicrobial activity of chitosan derivatives containing N-quaternized moieties in its backbone: a review. *Int. J. Mol. Sci.* **2014**, *15*, 20800−20832.

(2) Mano, J. F.; Silva, G. A.; Azevedo, H. S.; Malafaya, P. B.; Sousa, R. A.; Silva, S. S.; Boesel, L. F.; Oliveira, J. M.; Santos, T. C.; Marques, A. P.; Neves, N. M.; Reis, R. L. Natural origin biodegradable systems in tissue engineering and regenerative medicine: present status and some moving trends. *J. R. Soc., Interface* **2007**, *4*, 999−1030.

(3) Rodríguez-Vázquez, M.; Vega-Ruiz, B.; Ramos-Zúñiga, R.; Saldaña-Koppel, D. A.; Quiñones-Olvera, L. F. Chitosan and its potential use as a scaffold for tissue engineering in regenerative medicine. *BioMed Res. Int.* **2015**, *2015*, 821279.

(4) Valle Mendoza, L. J. d.; Franco García, M. L.; Katsarava, R.; Puiggalí Bellalta, J. Electrospun biodegradable polymers loaded with bactericide agents. *AIMS Mol. Sci.* **2016**, *3*, 52−87.

(5) Guo, Z.; Xing, R.; Liu, S.; Zhong, Z.; Ji, X.; Wang, L.; Li, P. Antifungal properties of Schiff bases of chitosan, N-substituted chitosan and quaternized chitosan. *Carbohydr. Res.* **2007**, *342*, 1329−1332.

(6) Umoren, S. A.; Banera, M. J.; Alonso-Garcia, T.; Gervasi, C. A.; Mirífico, M. V. Inhibition of mild steel corrosion in HCl solution using chitosan. *Cellulose* **2013**, *20*, 2529−2545.

(7) Gupta, N. K.; Joshi, P. G.; Srivastava, V.; Quraishi, M. A. Chitosan: A macromolecule as green corrosion inhibitor for mild steel in sulfamic acid useful for sugar industry. *Int. J. Biol. Macromol.* **2018**, *106*, 704−711.

(8) Jmiai, A.; El Ibrahimi, B.; Tara, A.; Oukhrib, R.; El Issami, S.; Jbara, O.; Bazzi, L.; Hilali, M. Chitosan as an eco-friendly inhibitor for copper corrosion in acidic medium: protocol and characterization. *Cellulose* **2017**, *24*, 3843−3867.

(9) Tian, H.; Li, W.; Liu, A.; Gao, X.; Han, P.; Ding, R.; Yang, C.; Wang, D. Controlled delivery of multi-substituted triazole by metal-organic framework for efficient inhibition of mild steel corrosion in neutral chloride solution. *Corros. Sci.* **2018**, *131*, 1−16.

(10) Dutta, A.; Saha, S. K.; Adhikari, U.; Banerjee, P.; Sukul, D. Effect of substitution on corrosion inhibition properties of 2-(substituted phenyl) benzimidazole derivatives on mild steel in 1 M HCl solution: a combined experimental and theoretical approach. *Corros. Sci.* **2017**, *123*, 256−266.

DOI: 10.1021/acsomega.8b00455
ACS Omega 2018, 3, 5654−5668

(11) El-Haddad, M. N. Chitosan as a green inhibitor for copper corrosion in acidic medium. *Int. J. Biol. Macromol.* **2013**, *55*, 142−149.
(12) Solomon, M. M.; Gerengi, H.; Kaya, T.; Kaya, E.; Umoren, S. A. Synergistic inhibition of St37 steel corrosion in 15% H_2SO_4 solution by chitosan and iodide ion additives. *Cellulose* **2017**, *24*, 931−950.
(13) Ahmed, R. A.; Farghali, R. A.; Fekry, A. M. Study for the stability and corrosion inhibition of electrophoretic deposited chitosan on mild steel alloy in acidic medium. *Int. J. Electrochem. Sci.* **2012**, *7*, 7270−7282.
(14) Srivastava, V.; Chauhan, D. S.; Joshi, P. G.; Maruthapandian, V.; Sorour, A. A.; Quraishi, M. A. PEG-Functionalized Chitosan: A Biological Macromolecule as a Novel Corrosion Inhibitor. *ChemistrySelect* **2018**, *3*, 1990−1998.
(15) dos Santos, J. E.; Dockal, E. R.; Cavalheiro, E. T. G. Synthesis and characterization of Schiff bases from chitosan and salicylaldehyde derivatives. *Carbohydr. Polym.* **2005**, *60*, 277−282.
(16) Jagadish, R. S.; Divyashree, K. N.; Viswanath, P.; Srinivas, P.; Raj, B. Preparation of N-vanillyl chitosan and 4-hydroxybenzyl chitosan and their physico-mechanical, optical, barrier, and antimicrobial properties. *Carbohydr. Polym.* **2012**, *87*, 110−116.
(17) Okoronkwo, A. E.; Olusegun, S. J.; Oluwasina, O. O. The inhibitive action of chitosan extracted from Archachatina marginata shells on the corrosion of plain carbon steel in acid media. *Anti-Corros. Methods Mater.* **2015**, *62*, 13−18.
(18) Liu, Y.; Zou, C.; Yan, X.; Xiao, R.; Wang, T.; Li, M. *β*-Cyclodextrin modified natural chitosan as a green inhibitor for carbon steel in acid solutions. *Ind. Eng. Chem. Res.* **2015**, *54*, 5664−5672.
(19) Sangeetha, Y.; Meenakshi, S.; SairamSundaram, C. Corrosion mitigation of N-(2-hydroxy-3-trimethyl ammonium) propyl chitosan chloride as inhibitor on mild steel. *Int. J. Biol. Macromol.* **2015**, *72*, 1244−1249.
(20) Menaka, R.; Subhashini, S. Chitosan Schiff base as effective corrosion inhibitor for mild steel in acid medium. *Polym. Int.* **2017**, *66*, 349−358.
(21) Haque, J.; Srivastava, V.; Verma, C.; Lgaz, H.; Salghi, R.; Quraishi, M. A. N-Methyl-N, N, N-trioctylammonium chloride as a novel and green corrosion inhibitor for mild steel in an acid chloride medium: electrochemical, DFT and MD studies. *New J. Chem.* **2017**, *41*, 13647−13662.
(22) Adejo, S. O.; Ekwenchi, M. M.; Gbertyo, J. A.; Menengea, T.; Ogbodo, J. O. Determination of adsorption Isotherm model best fit for methanol leaf extract of Securinega virosa as corrosion inhibitor for corrosion of mild steel in HCl. *J. Adv. Chem.* **2014**, *10*, 2737−2742.
(23) Sığırcık, G.; Yildirim, D.; Tüken, T. Synthesis and inhibitory effect of N, N-bis (1-phenylethanol) ethylenediamine against steel corrosion in HCl Media. *Corros. Sci.* **2017**, *120*, 184−193.
(24) Chauhan, D. S.; Ansari, K. R.; Sorour, A. A.; Quraishi, M. A.; Lgaz, H.; Salghi, R. Thiosemicarbazide and thiocarbohydrazide functionalized chitosan as ecofriendly corrosion inhibitors for carbon steel in hydrochloric acid solution. *Int. J. Biol. Macromol.* **2018**, *107*, 1747−1757.
(25) El Hamdani, N.; Fdil, R.; Tourabi, M.; Jama, C.; Bentiss, F. Alkaloids extract of Retama monosperma (L.) Boiss. seeds used as novel eco-friendly inhibitor for carbon steel corrosion in 1 M HCl solution: Electrochemical and surface studies. *Appl. Surf. Sci.* **2015**, *357*, 1294−1305.
(26) Srivastava, V.; Haque, J.; Verma, C.; Singh, P.; Lgaz, H.; Salghi, R.; Quraishi, M. A. Amino acid based imidazolium zwitterions as novel and green corrosion inhibitors for mild steel: Experimental, DFT and MD studies. *J. Mol. Liq.* **2017**, *244*, 340−352.
(27) Khadiri, A.; Saddik, R.; Bekkouche, K.; Aouniti, A.; Hammouti, B.; Benchat, N.; Bouachrine, M.; Solmaz, R. Gravimetric, electrochemical and quantum chemical studies of some pyridazine derivatives as corrosion inhibitors for mild steel in 1 M HCl solution. *J. Taiwan Inst. Chem. Eng.* **2016**, *58*, 552−564.
(28) Yousefi, A.; Javadian, S.; Dalir, N.; Kakemam, J.; Akbari, J. Imidazolium-based ionic liquids as modulators of corrosion inhibition of SDS on mild steel in hydrochloric acid solutions: experimental and theoretical studies. *RSC Adv.* **2015**, *5*, 11697−11713.
(29) Kowsari, E.; Arman, S. Y.; Shahini, M. H.; Zandi, H.; Ehsani, A.; Naderi, R.; PourghasemiHanza, A.; Mehdipour, M. In situ synthesis, electrochemical and quantum chemical analysis of an amino acid-derived ionic liquid inhibitor for corrosion protection of mild steel in 1 M HCl solution. *Corros. Sci.* **2016**, *112*, 73−85.
(30) Tian, H.; Li, W.; Hou, B.; Wang, D. Insights into corrosion inhibition behavior of multi-active compounds for X65 pipeline steel in acidic oilfield formation water. *Corros. Sci.* **2017**, *117*, 43−58.
(31) Wang, D.; Yang, D.; Zhang, D.; Li, K.; Gao, L.; Lin, T. Electrochemical and DFT studies of quinoline derivatives on corrosion inhibition of AA5052 aluminium alloy in NaCl solution. *Appl. Surf. Sci.* **2015**, *357*, 2176−2183.
(32) Hamani, H.; Douadi, T.; Al-Noaimi, M.; Issaadi, S.; Daoud, D.; Chafaa, S. Electrochemical and quantum chemical studies of some azomethine compounds as corrosion inhibitors for mild steel in 1 M hydrochloric acid. *Corros. Sci.* **2014**, *88*, 234−245.
(33) Yıldız, R. An electrochemical and theoretical evaluation of 4, 6-diamino-2-pyrimidinethiol as a corrosion inhibitor for mild steel in HCl solutions. *Corros. Sci.* **2015**, *90*, 544−553.
(34) Pearson, R. G. Chemical hardness—A historical introduction. *Chemical Hardness*; Springer, 1993; pp 1−10.
(35) John, S.; Joseph, A.; Sajini, T.; Jose, A. J. Corrosion inhibition properties of 1, 2, 4−Hetrocyclic Systems: Electrochemical, theoretical and Monte Carlo simulation studies. *Egypt. J. Pet.* **2017**, *26*, 721−732.
(36) Kokalj, A. Ab initio modeling of the bonding of benzotriazole corrosion inhibitor to reduced and oxidized copper surfaces. *Faraday Discuss.* **2015**, *180*, 415−438.
(37) Lgaz, H.; Salghi, R.; Bhat, K. S.; Chaouiki, A.; Shubhalaxmi; Jodeh, S. Correlated experimental and theoretical study on inhibition behavior of novel quinoline derivatives for the corrosion of mild steel in hydrochloric acid solution. *J. Mol. Liq.* **2017**, *244*, 154−168.
(38) Lgaz, H.; Bhat, K. S.; Salghi, R.; Shubhalaxmi; Jodeh, S.; Algarra, M.; Hammouti, B.; Ali, I. H.; Essamri, A. Insights into corrosion inhibition behavior of three chalcone derivatives for mild steel in hydrochloric acid solution. *J. Mol. Liq.* **2017**, *238*, 71−83.
(39) Kumar, R.; Chahal, S.; Kumar, S.; Lata, S.; Lgaz, H.; Salghi, R.; Jodeh, S. Corrosion inhibition performance of chromone-3-acrylic acid derivatives for low alloy steel with theoretical modeling and experimental aspects. *J. Mol. Liq.* **2017**, *243*, 439−450.
(40) Singh, A.; Ansari, K. R.; Haque, J.; Dohare, P.; Lgaz, H.; Salghi, R.; Quraishi, M. A. Effect of electron donating functional groups on corrosion inhibition of mild steel in hydrochloric acid: Experimental and quantum chemical study. *J. Taiwan Inst. Chem. Eng.* **2018**, *82*, 233−251.
(41) Quraishi, M. A.; Jamal, D. The influence of some condensation products on corrosion inhibition of mild steel in acidic solutions. *Anti-Corros. Methods Mater.* **2000**, *47*, 233−240.
(42) Obot, I. B.; Obi-Egbedi, N. O.; Ebenso, E. E.; Afolabi, A. S.; Oguzie, E. E. Experimental, quantum chemical calculations, and molecular dynamic simulations insight into the corrosion inhibition properties of 2-(6-methylpyridin-2-yl) oxazolo [5, 4-f][1, 10] phenanthroline on mild steel. *Res. Chem. Intermed.* **2013**, *39*, 1927−1948.
(43) Zhou, J.; Chen, S.; Zhang, L.; Feng, Y.; Zhai, H. Studies of protection of self-assembled films by 2-mercapto-5-methyl-1, 3, 4-thiadiazole on iron surface in 0.1 M H_2SO_4 solutions. *J. Electroanal. Chem.* **2008**, *612*, 257−268.
(44) Kokalj, A. Comments on the "Reply to comments on the paper "On the nature of inhibition performance of imidazole on iron surface" by JO Mendes and AB Rocha. *Corros. Sci.* **2013**, *70*, 294−297.
(45) Liu, A.; Ren, X.; Zhang, J.; Wang, C.; Yang, P.; Zhang, J.; An, M.; Higgins, D.; Li, Q.; Wu, G. Theoretical and experimental studies of the corrosion inhibition effect of nitrotetrazolium blue chloride on copper in 0.1 MH_2SO_4. *RSC Adv.* **2014**, *4*, 40606−40616.
(46) Xie, S.-W.; Liu, Z.; Han, G.-C.; Li, W.; Liu, J.; Chen, Z. Molecular dynamics simulation of inhibition mechanism of 3, 5-dibromo salicylaldehyde Schiff's base. *Comput. Theor. Chem.* **2015**, *1063*, 50−62.

DOI: 10.1021/acsomega.8b00455
ACS Omega 2018, 3, 5654−5668

(47) Standard, A., G1-03. Standard practice for preparing, cleaning, and evaluating corrosion test specimens. *Annual Book of ASTM Standards*, 2003; Vol. 3, pp 17−25.
(48) El Aal, E. E. A.; El Wanees, S. A.; Farouk, A.; El Haleem, S. M. A. Factors affecting the corrosion behaviour of aluminium in acid solutions. II. Inorganic additives as corrosion inhibitors for Al in HCl solutions. *Corros. Sci.* **2013**, *68*, 14−24.
(49) Ansari, K. R.; Quraishi, M. A.; Singh, A. Schiff's base of pyridyl substituted triazoles as new and effective corrosion inhibitors for mild steel in hydrochloric acid solution. *Corros. Sci.* **2014**, *79*, 5−15.
(50) *Materials Studio*, Revision 6.0; Accelrys Inc.: San Diego, United States, 2013.
(51) Delley, B. An all-electron numerical method for solving the local density functional for polyatomic molecules. *J. Chem. Phys.* **1990**, *92*, 508−517.
(52) Delley, B. From molecules to solids with the DMol 3 approach. *J. Chem. Phys.* **2000**, *113*, 7756−7764.
(53) Klamt, A.; Schüürmann, G. COSMO: a new approach to dielectric screening in solvents with explicit expressions for the screening energy and its gradient. *J. Chem. Soc., Perkin Trans. 2* **1993**, 799−805.
(54) Sánchez-Márquez, J.; Zorrilla, D.; Sánchez-Coronilla, A.; de los Santos, D. M.; Navas, J.; Fernández-Lorenzo, C.; Alcántara, R.; Martín-Calleja, J. Introducing "UCA-FUKUI" software: reactivity-index calculations. *J. Mol. Model.* **2014**, *20*, 2492.
(55) Yang, W.; Parr, R. G. Hardness, softness, and the fukui function in the electronic theory of metals and catalysis. *Proc. Natl. Acad. Sci., U.S.A.* **1985**, *82*, 6723−6726.
(56) Hu, S.-Q.; Guo, A.-L.; Yan, Y.-G.; Jia, X.-L.; Geng, Y.-F.; Guo, W.-Y. Computer simulation of diffusion of corrosive particle in corrosion inhibitor membrane. *Comput. Theor. Chem.* **2011**, *964*, 176−181.
(57) Yan, Y.; Wang, X.; Zhang, Y.; Wang, P.; Cao, X.; Zhang, J. Molecular dynamics simulation of corrosive species diffusion in imidazoline inhibitor films with different alkyl chain length. *Corros. Sci.* **2013**, *73*, 123−129.
(58) Sun, H. COMPASS: an ab initio force-field optimized for condensed-phase applications overview with details on alkane and benzene compounds. *J. Phys. Chem. B* **1998**, *102*, 7338−7364.
(59) Wu, R.; Qiu, X.; Shi, Y.; Deng, M. Molecular dynamics simulation of the atomistic monolayer structures of N-acyl amino acid-based surfactants. *Mol. Simul.* **2017**, *43*, 491−501.
(60) Hansen, J.-P.; McDonald, I. R. *Theory of Simple Liquids: With Applications to Soft Matter*, 4th ed.; Academic Press, 2013.

DOI: 10.1021/acsomega.8b00455
ACS Omega 2018, 3, 5654−5668